

Aerosol properties in a Chinese semiarid region

Xia Xiangao*, Chen Hongbin, Wang Pucai

LAGEO, Institute of Atmospheric Physics, Chinese Academy of Sciences, Dewai, Qijiahuozi, Chaoyang District, Beijing 100029, China

Received 19 December 2003; accepted 20 April 2004

Abstract

Aerosol optical properties and atmospheric water vapor content for 1999–2000 were obtained from ground-based solar radiometer measurements in Dunhuang, China. Seasonal changes of aerosol optical depth (AOD) and Angstrom wavelength parameter (ALPHA) were observed. Large values of AOD (at 500 nm) greater than 1.0 combined with low values of ALPHA less than 0.2 were mainly observed in spring and summer, which is consistent with the seasonal dust production from Gobi and Taklamaken deserts. The maximum monthly average of AOD was around 0.37 and occurred in the April of 1999, which was more than three times larger than the minimum monthly average in the November of 2000 (around 0.115). Thirty-three percent and 49% of observations of AOD in autumn and winter was larger than 0.2, respectively, whereas in spring, the percentage was approximately 63%. There was a large spread in ALPHAs in all seasons when AODs were less than 0.2. With the increase of AOD, ALPHAs decreased rapidly and were around zero finally. The large spread of ALPHA for low AODs and the domination of low turbidity in Dunhuang (nearly half of AODs less than 0.2) resulted in the negligible seasonal change of ALPHA. The domination of coarse particles over fine particles was also shown in aerosol size distribution retrievals, with the volume concentration ratio of coarse to fine particles being nearly 30. The volume mean radii and standard deviation of size distribution showed an insignificant correlation with AOD based on the analysis of all available retrievals, illustrating that it is suitable to use a fixed size model in the analysis of the dust climate forcing. During the dust outbreak episode, a rapid increase of AOD and a decrease of ALPHA were observed, ALPHA being usually less than 0.2 and even negative occasionally. The interesting result was that the volume mean radii of size distribution during the dust outbreak episode increased remarkably with the dust loading, which indicated that a dynamic size model should be used in the simulation of dust effects on meso-scale weather system in the semiarid region. The distinct seasonal change of water vapor content was observed, with high water vapor contents occurred in summer. The influence of water vapor on aerosol properties was absent due to the low humidification capability of dust aerosols and the different seasonal variation of aerosol properties and water vapor content.

© 2004 Elsevier Ltd. All rights reserved.

Keywords: Dust aerosol optical depth; Angstrom wavelength parameter; Size distribution; Dunhuang

1. Introduction

Aerosol radiative forcing remains one of the largest uncertainties in the simulation of climate system and the

projection of future climate change (IPCC, 2001). Much attention has been paid to anthropogenic sulfate aerosol, which has been believed to exert a substantial cooling influence and, to some extent, counteract the greenhouse effect. Dust aerosol effects on global climate have been thought to be generally insignificant due to its deemed low-scattering efficiency and short lifetime (Charlson et al., 1992). However, observations in

*Corresponding author. Tel.: +86-10-62048922; fax: +86-10-62046349.

E-mail address: xxa@mail.iap.ac.cn (X. Xiangao).

Barbados suggested that dust aerosol was an important climatic forcing agent in source and downwind regions due to its dominant concentrations over other aerosols (Li et al., 1996). On the global scale, three major components: sulfate, dust and carbonaceous particles, appeared to contribute equally to the column-integrated total optical depth (Tegen et al., 1997). Great progresses have been made recently with regard to the dust aerosol radiative forcing due to much attention having been paid to this issue; however, we need to admit that we are far from the full understanding of the role dust plays in the climate system. Considerable uncertainties in the estimation of dust radiative forcing were highlighted in the latest IPCC assessment report (Intergovernmental Panel on Climate change, IPCC, 2001). This is in part due to our poor understanding of dust aerosol properties and their spatial and temporal variation. Hence, it is significant to obtain such information via all possible channels.

Ground-based remote sensing of aerosols is best suited to reliably and continuously derive detailed aerosol properties in key locations partly due to its larger information content compared with the spaceborne remote sensing. An automatic robotic sun and sky scanning measurement program (AERONET) has grown rapidly through international federation since 1993 to over 100 sites worldwide so far. The program provides the satellite remote sensing, aerosol, land and ocean communities quality-assured aerosol optical properties to assess and validate satellite retrievals (Holben et al., 2001). AERONET has also played an important role in the characterization of key aerosol types: urban–industrial aerosol, biomass burning aerosol, desert dust and marine aerosol (Holben et al., 2001; Dubovik et al., 2002; Eck et al., 2001; Pinker et al., 2001; Smirnov et al., 2002a,b). A sun/sky radiometer network based in East-Asia (SKYNET) was also established and provides similar measurements as AERONET (Takamura et al., 2002).

Gobi and deserts over northwest China are one of principal dust source regions in East Asia. Intense frontal activities in spring provide a mechanism for the injection of substantial materials into the lower and middle troposphere. It is estimated that nearly 800 Tg/a (with an uncertainty of approximately 40%) of mineral aerosols are emitted into the atmosphere each year, among which 50% is deposited over the source and adjacent regions and the remainder is transported to the remote Pacific Ocean (Zhang, 2001). Information on Chinese dust properties and their spatial and temporal variation are still limited despite dust has been playing an important role in climate and atmospheric environment. The objective of this study is to characterize the dust aerosol and water vapor content of the atmosphere in a Chinese semi-arid region based on continuous spectral solar direct and scattering radiance measure-

ments by a sun/sky radiometer for 1999–2000. Although short-term observations have been attempted in Western China (Wang and Qiu, 1986), such a multiyear record of aerosol observations made during conditions ranging from very clean to very dusty should provide us a valuable data set to improve the knowledge of aerosol properties in Chinese dust source regions.

2. Site description

Solar direct and sky radiance measurements presented in this paper were made from January 1999 to November 2000 in Dunhuang (DH: Latitude: 40.04°; Longitude: 94.79°; Altitude: 1300 m), a tiny oasis rounded by high mountains, desert and Gobi, with the averaged altitude of 1100 m. DH is located at the west end of Hexi Corridor of Gansu province of China, which is one of dust activity centers in China. Due to its special location and good infrastructure, DH has been established as one of the super-sites for many international aerosol field experiments, for instance, the Aerosol Characterization Experiment—Asia (ACE—Asia), China and Japan joint plan on Aeolian dust effect on climate (ADEC). Due to in the depths of Inland China, DH has a very dry climate with lots of direct sunshine. The annual averaged rainfall here is only 39.9 mm and approximately 63.9% of rainfall concentrates in summer, while winter rainfall is only 7.5%. The annual average of temperature is 9.3°C and with huge annual and daily difference. The monthly average of wind speed is about 2 m/s, with large values occurred in spring. The combination of the special location, the earth's surface condition, as well as its dry and windy climate causes that DH is frequently affected by dust storms in spring and summer (Zhou, 2001).

3. Instrument and measurement

A sun/sky radiometer (also called Aureolemeter) Model Pom-01, produced by Prede is utilized in the measurements. The radiometer uses the following wavelengths (315, 400, 500, 675, 870, 940, 1020 nm) to detect direct and scattering radiation with the same detector, which has dynamic range of 10^7 . As for filters, the half bandwidths of 315 is 2 nm, while for the other band pass, it is close to 10 nm. The field of view is 1° and the minimum angle for scattering measurements is about 3°. The photometer is mounted on a vertical-horizontal two-axis mount that is driven by digital servomotors to carry out sky radiance almucantar measurements. A preprogrammed sequence of measurements is taken by aureolemeter: during periods of air mass larger than 3, solar direct and scattering measurements are made at

about 0.25 air mass intervals, while at smaller air masses, the interval is typically 10 min.

4. Data-processing methodology

4.1. Calibration of radiometer

It is essential in ground-based measurements to calibrate accurately radiometer constant (Schmid et al., 1998). The accuracy with which AODs can be retrieved depends mainly on the accuracy of the $V_{0,\lambda}$ value. The error of $V_{0,\lambda}$ should be less than 2% in order to obtain AOD with an uncertainty less than 0.02 when the air mass is equal to 1. The Langley method (LM) that is a straightforward application of the Bouguer–Lambert–Beer law is practically the de facto standard, owing to its high accuracy and being convenient to be undertaken in the field.

$$V_{\lambda} = V_{0,\lambda} d^{-2} \exp(-\tau_{\text{t}} m),$$

where λ is filter wavelength, V_{λ} , $V_{0,\lambda}$ depict the radiometer measurement at the surface and the its response at the space at a given wavelength, d is the Earth–Sun distance in astronomical units at the time of observation, τ_{t} is total optical depth including molecular scattering, aerosol extinction and ozone absorption. For the wavelength at 940 nm, in addition to the Beer's law extinction contribution of aerosol and molecular scattering to the total optical thickness, there is an extinction contribution from water vapor that departs from the Beer's law. Hence, the equation mentioned above becomes:

$$V_{940} = V_{0,940} d^{-2} \exp(-\tau_{\text{total}} m - k(Wm)^b),$$

where W is vertical-integrated water vapor content in cm, and k and b are experiential coefficients obtained from numerous simulation experiments (Zhu and Zhou, 1998; Schmid et al., 2001).

The assumption made by LM is that atmosphere remains stable during the calibration period of one to several hours. However, this is not satisfied at most locations and under most situations. Accordingly, some modified Langley methods (MLMs) have been developed (Tanaka et al., 1986; O'Neill and Miller, 1984), in which temporarily variable atmospheric turbidity was taken into consideration. Aureole intensity measurements are preferred to provide such information because they are approximately proportional to the atmospheric turbidity. The common feature of these methods is that the relative aerosol size distribution and optical properties are assumed to remain constant, but the absolute size distribution is permitted to vary during the calibration period. Nakajima et al. (1996) extended Tanaka's method (MLM): Firstly, an inversion with only forward scattering intensity data (3–30°) is

performed. Then derived temporarily variable aerosol optical depths (AOD) are multiplied by the corresponding air mass (m) and used to derive values of the abscissa for a $V-m\tau_{\text{a}}$ scattering graph. Finally, the radiometer constant is obtained through a linear fit of the data points. More accurate calibration is expected since this extension allows the relative size distribution to vary with time; hence, MLM is used in the study to calibrate the radiometer.

4.2. Calculation of AOD, Angstrom wavelength exponent (ALPHA)

Based on the radiometer constant calibration, the atmospheric optical depth except at the wavelength of 940 nm can be calculated according to the Beer–Lambert–Bouguer law

$$\tau_{\text{t}} = \tau_{\text{a}} + \tau_{\text{r}} + \tau_{\text{O}_3} = -\frac{1}{m} \ln\left(\frac{V_{\lambda}}{V_{0,\lambda}}\right).$$

The atmosphere optical depth (τ_{t}) is the sum of τ_{a} (AOD), τ_{r} , Rayleigh scattering depth and τ_{O_3} , ozone absorption depth. The latter two are calculated from equations below (Nakajima et al., 1996)

$$\tau_{\text{r}} = 0.00864/\lambda^{(3.916+0.074\times\lambda+0.05/\lambda)} \times \text{PRS},$$

$$\tau_{\text{O}_3} = a \times \text{O}_3,$$

where PRS represents the surface pressure measured in DH Meteorological Observatory, the coefficient a represents the ozone absorption coefficient. O_3 is the ozone column amount from daily total ozone mapping spectrometer (TOMS) observation.

ALPHA, which is a measure of the wavelength dependence of AOD and therefore sensitive to particle size distribution and indicative of different types of aerosol particle composition, is computed from the AOD data within the radiometer wavelength range. The linear regression is carried out for five wavelengths (400, 500, 675, 870, 1020 nm) and corresponding AODs at the logarithmic scale to compute ALPHA.

4.3. Inversion of aerosol size distribution

A combination of solar direct and scattering radiance measurement was utilized to invert aerosol size distribution based on SKYRAD software developed by Nakajima et al. (1996). They described the structure of model and evaluated the retrieval precision in detail. A brief description is, however, provided here for completeness. The code is composed of two parts: the first is improved multiple scattering radiative transfer scheme (IMS) in a plane-parallel atmosphere developed by Nakajima and Tanaka (1986), and the second part is the inversion scheme. On an average, the errors for the minimum and maximum size ranges (0.05–0.1 μm and 7–

15 μm) may be as large as 35–100%, but the precision for the middle range is expected to be within 80%. The forward scattering range (scattering angles from 3° to 30°) is utilized to invert size distribution due to negligible non-spherical effects and little influences from uncertainties in refractive index and surface albedo on retrievals within these range, as suggested by Kaufman et al. (1994).

4.4. Cloud screening of data

For the manual observations, it is in principle not difficult to carry out the data screening. Experienced human observer can detect cloud according to the textual and spatial pattern, and then eliminate disturbed data points. The automatic radiometer collects data according to the preprogrammed sequence regardless of sky conditions, except in rainy days, thus the cloud screening is essential for the data quality. Here, the cloud screening method developed by Smirnov et al. (2000) was utilized firstly to eliminate artificial observations. This technique relies on the principle that cloud has greater temporal variance compared with aerosol. Diurnal stability and smoothness checks were performed according to the description of Smirnov et al. (2000). Additionally, the measurements at a given wavelength with a deviation from a second-order polynomial fit to the $\ln \tau_a$ versus $\ln \lambda$ greater than 0.02 are rejected. This is due to that a second-order polynomial fit between AOD and wavelength in the logarithmic space can give an excellent agreement with differences of the same order as the measurement uncertainty in AOD (approximately 0.01–0.02) (Eck et al., 1999). Lastly, the manual cloud screening for the questionable data was performed depending on the weather observations from DH Observatory.

5. Results

5.1. Radiometer calibration result

An example of calibration is presented in Fig. 1, which was based on the observations on 6 April 2000. There was a large difference between the calibrations in the morning and the afternoon when LM was used, evidently, it was artificial since the calibrations were carried out at the same day, so the similar results should be obtained. The good agreement was achieved when MLM was used as shown in Fig. 1. The temporal variation of radiometer constant calibrations on the basis of MLM normalized to an Earth–Sun distance of 1 AU is shown in Fig. 2 for six wavelengths. It was shown that the calibration of the radiometer constant had a small temporal variation, with a relative standard deviation of 4.7%, 6.7%, 3.5%, 4.0% and 4.5% at the

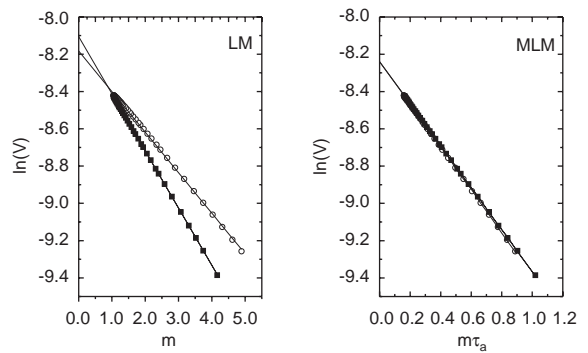


Fig. 1. Calibration results by using of the LM and the MLM based on radiometer measurements on 6 April, 2000. The large difference (top) in the calibrations at the same day (in the morning and afternoon) indicates the temporal variation of turbidity deteriorate the calibration if LM is used; however, MLM produces a good consistency in the calibrations (bottom).

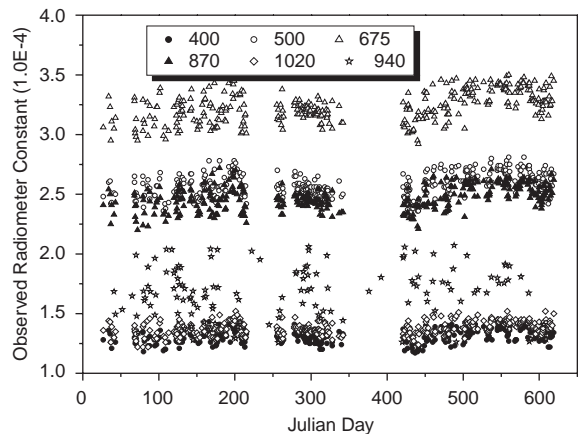


Fig. 2. Times series of radiometer constants derived from MLM and normalized to 1 AU at six filters.

wavelength of 400, 500, 675, 870 and 1020 nm, respectively; however, the calibration derived by the general LM showed much higher temporal variation, with a relative standard deviation of an order of magnitude larger than MLM. The results demonstrated that there was little instrument degradation possibly caused by the soiling of the diffuser or filter transmission changes. This is remarkable considering that DH is often affected by frequent dust events. The largest temporal variation appeared at the wavelength of 940 nm. This is due to the extra condition is required: water vapor content should remain stable during the calibration period other than the stable aerosol content. The individual calibration is always associated with unacceptable errors. Fortunately, these errors are not systematic in nature, so it is expected that the accuracy

can be improved by averaging or calculating median providing that the instrument's response remains stable for the averaging period (Harrison and Michalsky, 1994). Accordingly, the average of a group of continuous 40 successful modified Langley calibrations that are near in time to the day for which a constant is required is used to derive AODs.

5.2. Aerosol loading and size

Fig. 3 displays the full cloud-screened daily average of AOD data at 500 nm, also included is the daily TOMS/aerosol index (AI) (see the dedicated introduction by Herman et al. (1997) with regard to TOMS/AI). AODs showed a significant seasonal variation in this arid area with high values mainly occurred in spring, then in summer. The maximum monthly average of AOD (0.37 with one standard deviation of 0.13) occurred in April of 1999, which was actually more than three times larger than the minimum occurred in November of 2000 (0.115 with one standard deviation of 0.029). AOD averages in autumn and winter were only 59% and 65% of that in spring, respectively (see Table 1). The obvious seasonal variation of AOD was also observed in other western stations such as Germu and Waliguan in the study of Zhang et al. (2002) and Qiu and Yang (2000). Most importantly, it might also be supported by the analysis of long-term surface weather report data, which suggests that frequent dust events in the Hexi Corridor occur

mostly in spring and summer (Zhou, 2001). The good consistency between high AODs and TOMS/AI as shown clearly in Fig. 3 illustrated a good agreement in the detection of dust outbreaks by use of AODs and TOMS/AI in Chinese dust source regions. Despite that there were a little spread based on the analysis of individual daily observations of TOMS/AI and AOD (this probably resulted from the large spatial and temporal variation of aerosol and the inexact collocation between TOMS/AI and AOD), the sound linear correlation between each TOMS/AI value (the interval of TOMS/AI is 0.05) and the corresponding average of AODs was evident in Fig. 4 ($r=0.89$). This is indicated that TOMS/AI may also play the same important role in the research on detecting dust source, monitoring transportation and dust climate forcing in Chinese dust source regions as that in Sahara (Hsu et al., 1999). The maximum monthly average of AOD (0.37) was much lower than that in the urban region such as in Miyun, Beijing's suburb (0.56 in June of 1998) and in Xinfeng (0.60 in April of 1998) (Zhang et al., 2002), which indicated that the anthropogenic production might be dominant over the natural emission in China. But it is worth mentioning that the large temporal variance of desert dust AOD at DH is possible since the site is so near to a very strong source region, and that this temporal variance may result in some large AOD events being screened as cloud. As seen in Fig. 5, however, ALPHA showed little seasonal variation, with

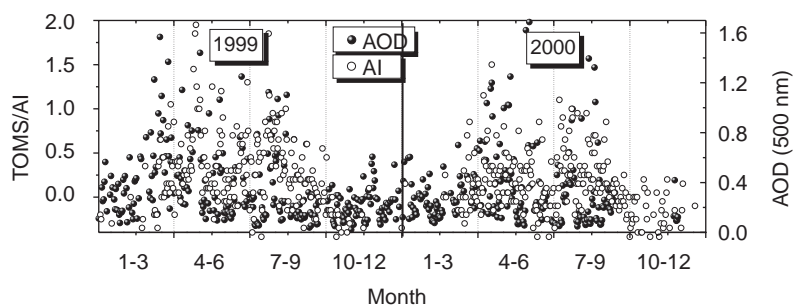


Fig. 3. Daily averages of ground-based measurements of AOD at 500 nm and TOMS derived AI (TOMS/AI).

Table 1
The monthly average of AOD and ALPHA and one standard deviation

Month		Jan	Feb	Mar	Apr	May	Jun	Jul	Aug	Sep	Oct	Nov	Dec
1999	AOD	0.26	0.24	0.29	0.37	0.23	0.25	0.23	0.19	0.16	0.19	0.19	0.22
	Std	0.17	0.16	0.12	0.13	0.12	0.12	0.15	0.09	0.11	0.12	0.12	0.14
	ALPHA	0.25	0.01	0.22	0.17	0.44	0.16	0.22	0.21	0.20	0.30	0.18	0.10
	Std	0.20	0.14	0.16	0.14	0.42	0.14	0.2	0.12	0.15	0.27	0.20	0.17
2000	AOD	0.19	0.23	0.29	0.29	0.29	0.30	0.20	0.14	0.25		0.12	
	Std	0.08	0.12	0.19	0.21	0.35	0.35	0.16	0.10	0.10		0.03	
	ALPHA	0.36	0.33	0.21	0.26	0.20	0.35	0.5	0.66	0.32		0.32	
	Std	0.17	0.23	0.16	0.21	0.22	0.33	0.27	0.48	0.14		0.15	

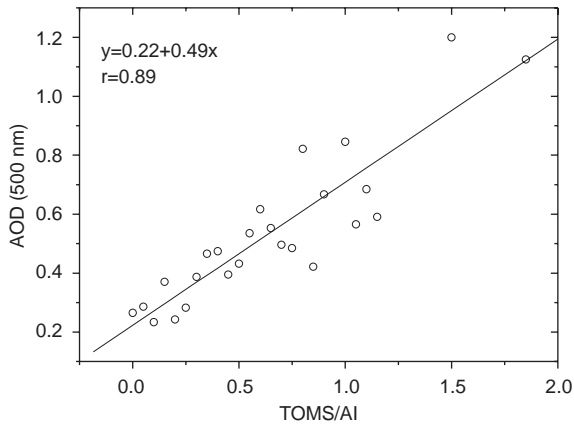


Fig. 4. Linear correlation analysis between each TOMS/AI value (the interval of TOMS/AI is 0.025) and corresponding average of AODs.

high values mainly occurred at the two ends of the measurement period. Generally, the monthly average of ALPHA is nearly 0.2, which was also much lower than that in Miyun and Xinfeng (Zhang et al., 2002).

Fig. 6 depicts the histograms of daily AODs at 500 nm and ALPHA for each season. It is more suitable to depict AOD histogram by the lognormal probability distribution than a normal probability distribution; however, the normal probability distribution is a better representation of ALPHA histogram, which is consistent with O'Neill et al. (2000) results. Hence, the geometric mean and standard deviation are more appropriate for AOD statistics than the arithmetic average and deviation. Even though DH is frequently affected by dust events, nearly half of AODs was smaller than 0.2 (the largest and smallest percentage occurred in autumn and spring, respectively). Approximately 8.5% of ALPHA was negative, indicative of anomalous

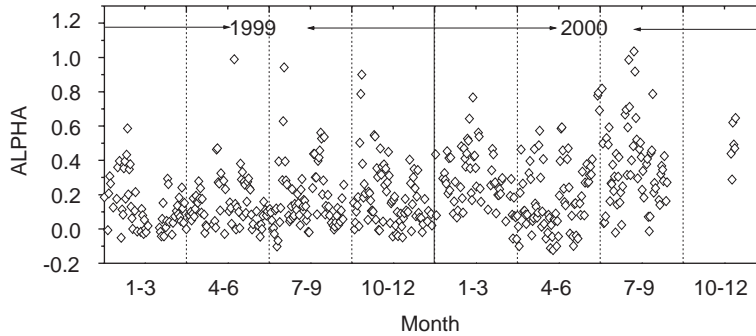


Fig. 5. Daily averages of ground-based measurements of ALPHA.

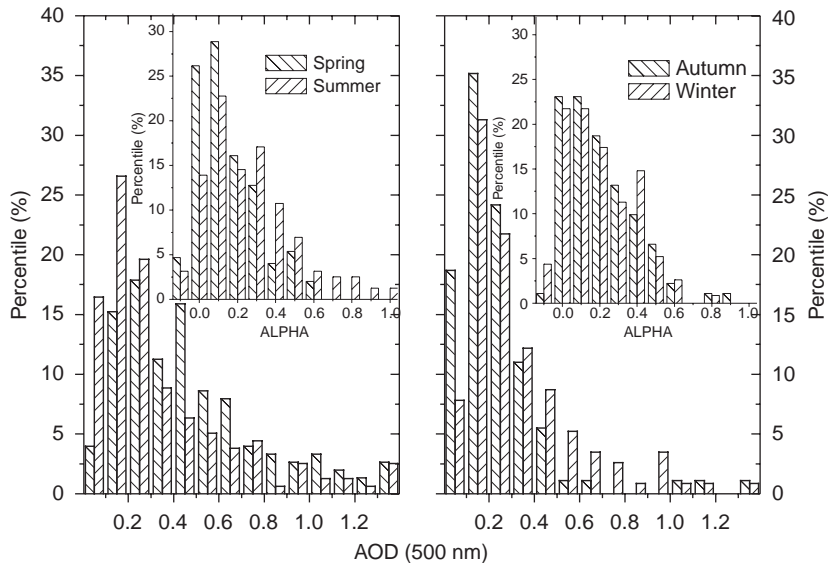


Fig. 6. The histogram of daily AOD at 500 nm and ALPHA for each season in Dunhuang (left. Spring and summer; right. Autumn and winter). The same scale is utilized to demonstrate seasonal difference of AOD and ALPHA.

extinction; the largest frequency occurred in winter, that was 16%. Wang and Qiu (1986) also observed the dust anomalous extinction during a dust outbreak episode in the Tarimu Basin. More than 50% of ALPHA in DH was less than 0.2. Fig. 7 presents the scatter plots of ALPHA and AOD at 500 nm for four seasons. All seasons showed a similar dependence of ALPHA on AOD. There was a large spread of ALPHA varying from negative to 2 for small AOD (<0.2), and then ALPHA remained below 0.5 for the intermedian AOD range (0.2 < AOD < 0.75), whereas ALPHAs were around zero for large AOD values (>0.75), which mainly appeared in spring and summer. A wide spread

of ALPHA at moderate to low AOD was also observed in other dust source regions (Smirnov et al., 2002a, b). A combination of domination of low turbidities in DH (approximately 50% of AODs at 500 nm is below 0.2) and a large spread of ALPHA under low turbidities as shown in Fig. 7 resulted in little seasonal variation of ALPHA in DH. The seasonal average of volume size distribution retrievals also supports the observed little seasonal variation of ALPHA. Fig. 8 presents the seasonal average of aerosol volume size distribution retrievals normalized to one AOD at 500 nm (left) and size distribution retrievals for AOD at 500 nm varying from 0.10 to 0.50 (each size distribution was the average

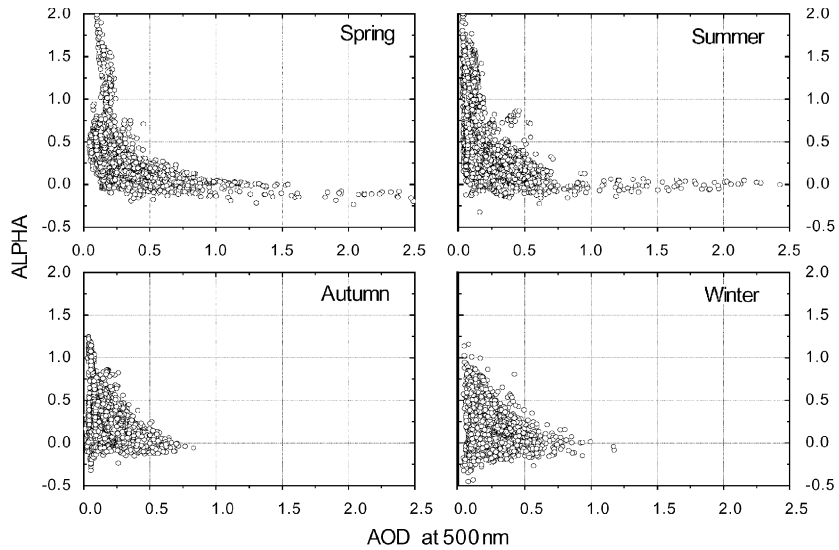


Fig. 7. The scatter plots of instantaneous ALPHA versus AOD at 500 nm for each season. The same scale is utilized to demonstrate the seasonal difference of AOD and ALPHA.

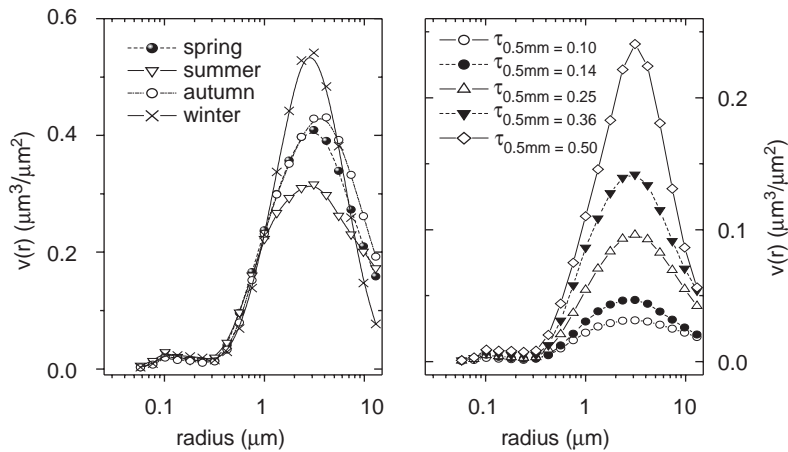


Fig. 8. Aerosol size distribution retrievals in four seasons (normalized to one AOD at 500 nm) (left) and size distribution retrievals for AOD at 500 nm varying from 0.10 to 0.50.

computed from at least 40 individual retrievals). Generally speaking, the mean size distributions were bimodal in shape and could be represented as

$$v(r) = \frac{dV(r)}{d \ln r} = \sum_{i=1}^2 \frac{C_{v,i}}{\sqrt{2\pi}\sigma_i} \exp\left[-\frac{(\ln r - \ln r_{v,i})^2}{2\sigma_i^2}\right],$$

where $v(r)$ is the volume distribution, $C_{v,i}$ is the volume concentrations for fine ($r < 0.6 \mu\text{m}$) and coarse ($r > 0.6 \mu\text{m}$) mode per cross-section of an atmospheric column, r is the aerosol radius, $r_{v,i}$ is the volume median radius, and σ_i is the geometric standard deviation for each mode. These integrated quantities of aerosol size distribution can be calculated approximately as suggested by Dubovik et al. (2002).

The principal feature of size distribution retrievals was the domination of large particles, with the volume concentration ratio of coarse to fine modes being 30. The ratio is lower than that in Sahara and Middle East (~ 50), but higher than that in Bahrain Persian Gulf (Dubovik et al., 2002). Seasonal r_{vf} was approximately $0.20 (\pm 0.04) \mu\text{m}$ and varied little, as for r_{vc} , similarly, little seasonal variation was observed, being 2.75 ± 0.49 ; 2.74 ± 0.27 , 2.69 ± 0.30 , $2.79 \pm 0.38 \mu\text{m}$ in spring, summer, autumn, and winter, respectively. The mode radii were slightly larger than the retrievals in Sahara and Middle East ($r_{vf} \sim 0.12\text{--}0.15 \mu\text{m}$ and $r_{vc} \sim 1.9\text{--}2.54 \mu\text{m}$) (Dubovik et al., 2002); however, Pinker et al. (2001) observed r_{vc} with $\sim 4 \mu\text{m}$ in sub-Sahel region. The dynamic response of mode radii and standard deviation to AOD was absent. This is consistent with measurements in other dust source regions (Dubovik et al., 2002). The lack of a close relation between the mode radii of fine and coarse mode with AOD suggested that a fixed dust size model was suited in the study of the dust climate forcing.

Notable seasonal variation of water vapor content was obvious from Fig. 9, with high values mainly occurred in summer, which was consistent with the description of the climate in DH. AOD and ALPHA had little correlation with water vapor content (relation coefficient less than 0.1), which was contrary to the observed increase of r_{vf} with AOD for urban and smoke aerosols (Holben et al., 2001). This is due partly to the very weak humidification capability of dust, as compared with urban or smoke aerosols, additionally, the distinctly difference in seasonal variation of AOD, ALPHA and water vapor content also prevents the occurrence of a close relation between AOD, ALPHA and water vapor content.

5.3. Dust property variation during a dust outbreak episode

The mode radii show little correlation with AOD as discussed in the above section, and then the next

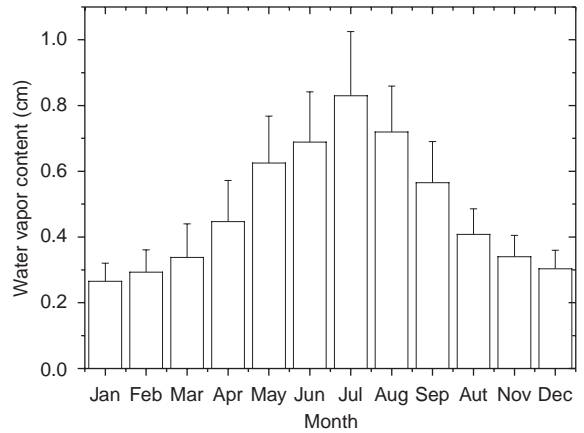


Fig. 9. Monthly means of water vapor content with one standard deviation depicted by the short bar.

question will arise naturally, that is, whether the dust mode radii remain stable during the dust outbreak episode? It was reported that the dust heating (the difference between the dust absorption of solar and thermal radiation and the dust emission) played an important role in the development of the dust event, and that the dust heating was associated with dust size (Chen et al., 1995). We will focus on this issue based on the observations during a dust episode. Surface weather reports showed that during the period from 6 April 2000 to 14 April 2000, a few dust events took place in DH. The first blowing dust event was reported at 0800 LST 7 April, with visibility decreasing from 30 km the day before to 9 km. Persistent dust events were reported on 9 April, at 1100, 1400, 1700 and 2000 LST, respectively, with visibility less than 10 km. The last floating dust record occurred at 1400 LST 10 April. Fortunately, ground cloud observations and Geostationary Meteorological Satellite (GMS) cloud maps showed that a clear sky condition was dominant in the daytime except on 12 April. This ensured sufficient surface based and satellite measurements free from cloud contamination. Fig. 10 presents instantaneous AOD at 500 nm and ALPHA. Preceding flowing dust on 7 April, AODs were relatively stable, having value of ~ 0.15 , and ALPHA ranged from 0.2 to 0.4. With the advent of dust event, AODs increased rapidly to ~ 0.5 on 7 April and maintained this value on 8 April. AODs increased dramatically when persistent blowing and floating dust events occurred on 9 April, with the maximum of AOD approaching 2.0. The persistent high turbidity continued to the subsequent two days. Until 13 April, atmosphere returned to the low turbidity with AOD of ~ 0.15 . The increase of dust loading was combined with a decrease of ALPHA as shown by Fig. 10. Corresponding to the high aerosol loading on 9 April and 10 April, nearly all ALPHAs were close to zero, with a few values even

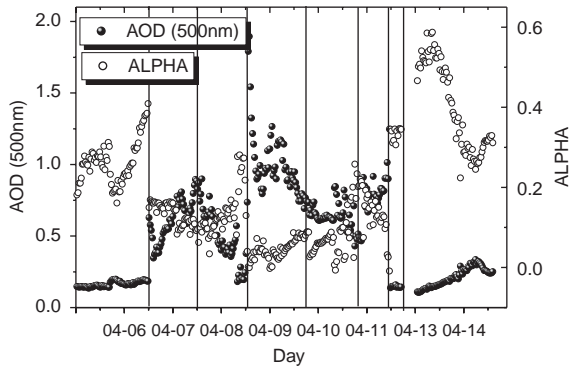


Fig. 10. Time series of AOD and ALPHA from 6 April to 14 April, 2000. The abrupt variation of AODs occurred preceding and ending the dust event. The peak AODs approached to nearly 2.0 on 9 April, correspondingly, the ALPHAs decreased to nearly zero, even to negative value occasionally, indicating that the elevated aerosol concentrations are caused dominantly by large dust particles.

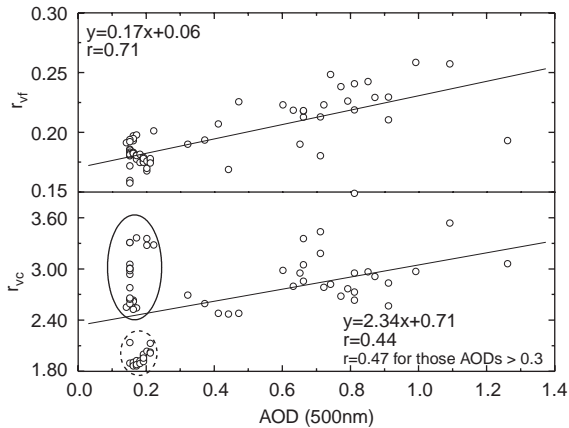


Fig. 11. The scattergram between the mode radii and AOD at 500 nm (top: fine mode; bottom: coarse mode) during the dust outbreak episode. The dots surrounded by the dash and solid circle at the bottom figure, represented observations preceding and ending the dust outbreak, respectively. The increasing mode radii with AOD were evident.

negative occasionally. Fig. 11 presents the scatter plots between AOD and the volume median radius of fine and coarse modes. A significant positive correlation between r_{vf} and AOD was evident, with approximately 50% deviation of r_{vf} being accounted for by AOD. It seemed more primary fine particles with larger size were injected into the atmosphere during the dust outbreak episode since the dust hygroscopic growth was very weak. As for r_{vc} , the points are distributed widely in the scatter plot: especially for lower AODs than 0.2, r_{vc} varied at 100%.

However, it should be pointed that the large spread was mainly resulted from the large difference in r_{vc} preceding and ending the dust outbreak. Anyway, the general trend was that the dust outbreak could result in a larger mode radius than the normal. Obviously, this was not consistent with the result presented in the Section 5.2, which suggested that a dynamic size model should be used in the simulation of the dust heating during the dust outbreak episode.

6. Conclusions

Two years of solar direct and sky radiance measurements in DH have been utilized to invert aerosol optical and physical properties as well as water vapor content. It is believed to be the first similar attempt in Chinese dust source regions as those carried out in Sahara and other aerosol hot spots. Based on elaborated radiometer calibrations and sound data screening methods, the seasonal change of aerosol properties such as AOD, ALPHA, aerosol volume size distribution, as well as water vapor content were derived.

Higher AODs at 500 nm than 0.75 occurred mostly in spring and summer, which corresponded to the frequent occurrence of dust events in DH. The average of AOD in autumn and winter was only about 60% of that in spring. ALPHA showed negligible seasonal change due in part to high percentage of the low turbidity and a large spread of ALPHA for median and low AODs. Aerosol size distribution retrievals showed little seasonal variation, which supported the negligible seasonal ALPHA variation. Aerosols in DH were dominated by large particles, with the volume concentration ratio of coarse mode to fine modes being 30. The significant correlation between aerosol properties and water vapor content was not observed. All these features demonstrated that aerosols in DH seemed to have properties representative of so-called pure desert dust. A fixed size model might be used in the analysis of the dust effect on climate due to an insignificant correlation between the aerosol loading and the volume mean radii of size distribution, contrarily; a dynamical size model should be taken in the simulation of the dust heating on the atmosphere during the dust outbreak episode.

The accumulation of these measurements is absolutely necessary for the study on the dust aerosol radiative forcing, validation of satellite remote sensing and aerosol transport models, as well as the atmospheric retrieval and correction algorithms.

Acknowledgements

The research is supported by NSFC (40305002, 40175008, and 40028503). Support from M. Yamano,

Prof. Takamura, as well as Prof. G. Y. Shi in site management and data processing was greatly appreciated. The authors thank Prof. Nakajima for providing SKYRAD software. Supply of TOMS/AI data by NASA is also appreciated. We thank the anonymous reviewers for their constructive comments and their help in modifying English.

References

- Charlson, R.J., Schwartz, S.E., Hales, J.M., Cess, D., Coakley, J.A., Hansen, J.E., 1992. Climate forcing by anthropogenic aerosols. *Science* 255, 423–430.
- Chen, S.J., Kuo, Y.H., Ming, W., Ying, H., 1995. The effect of dust radiative heating on low-level frontogenesis. *Journal of the Atmospheric Sciences* 52, 1414–1420.
- Dubovik, O., Holben, B., Eck, T.E., Smirnov, A., Kaufman, Y.J., King, M.D., Tanré, D., Slutsker, I., 2002. Variability of absorption and optical properties of key aerosol types observed in worldwide locations. *Journal of the Atmospheric Sciences* 59, 590–608.
- Eck, T.F., Holben, B.N., Reid, J.S., Dubovik, O., Smirnov, A., O'Neill, N.T., Slutsker, I., Kinne, S., 1999. Wavelength dependence of the optical depth of biomass burning, urban, and desert dust aerosols. *Journal of Geophysical Research* 104, 31,333–31,349.
- Eck, T.F., Holben, B.N., Reid, J.S., Dubovik, O., Smirnov, A., Slutsker, I., Lobert, J.M., Ramanathan, V., 2001. Column-integrated aerosol optical properties over the maldives during the northeast monsoon for 1999–2000. *Journal of Geophysical Research* 106, 28,555–28,566.
- Harrison, L., Michalsky, J., 1994. Objective algorithms for the retrieval of optical depths from ground-based measurements. *Applied Optics* 33, 5126–5132.
- Herman, J.R., Bhartia, P.K., Torres, O., Hsu, N.C., Seftor, C.J., Celarier, E., 1997. Global distribution of UV-absorbing aerosols from nimbus 7/TOMS data. *Journal of Geophysical Research* 102, 16,911–16,921.
- Holben, B.N., Tanré, D., Smirnov, A., Eck, T.F., Slutsker, I., Abuhassan, N., Newcomb, W.W., Schafer, J.S., Chatenet, B., Lavenu, F., Kaufman, Y.J., Vande, C.S.A., Markham, B., Clark, D., Frouin, F., Halthore, R., Karneli, A., O'Neill, N.T., Pietras, C., Pinker, R.T., Voss, K., Zibordi, G., 2001. An emerging ground-based aerosol climatology: aerosol optical depth from AERONET. *Journal of Geophysical Research* 106, 12,067–12,097.
- Hsu, N.C., Herman, J.R., Torres, O., Holben, B.N., Tanre, D., Eck, T.F., Smirnov, A., Chatenet, B., Lavenu, F., 1999. Comparisons of the TOMS aerosol index with Sun-photometer aerosol optical thickness: results and applications. *Journal of Geophysical Research* 104, 6269–6279.
- Intergovernmental Panel on Climate Change (IPCC) 2001. *Climate Change 2001: The Scientific Basis-Contribution of Working Group I to the Third Assessment Report of the Intergovernmental Panel on Climate Change*. Cambridge University Press, New York.
- Kaufman, Y.J., Gitelson, A., Karnieli, A., Ganor, E., Fraser, R.S., Nakajima, T., Mattoo, S., Holben, B.N., 1994. Size distribution and phase function of aerosol particles retrieved from sky brightness measurements. *Journal of Geophysical Research-Atmospheres* 99, 10,341–10,356.
- Li, X.H.M., Savoie, D., Voss, K., Prospero, J.M., 1996. Dominance of mineral dust in aerosol light-scattering in the north atlantic trade winds. *Nature* 380, 416–419.
- Nakajima, T., Tanaka, M., 1986. Matrix formulations for the transfer of solar radiation in a plane-parallel scattering atmospheric. *Journal of Quantitative Spectroscopy and Radiative Transfer* 35, 13–21.
- Nakajima, T., Tonna, T., Rao, R., Kaufman, Y., Holben, B., 1996. Use of sky brightness measurements from ground for remote sensing of particulate polydispersions. *Applied Optics* 35, 2672–2686.
- O'Neill, N.T., Miller, J.R., 1984. Combined solar aureole and solar beam extinction measurements. I: calibration considerations. *Applied Optics* 23, 3691–3696.
- O'Neill, N.T., Ignatov, A., Holben, B.N., Eck, T.F., 2000. The lognormal distribution as a reference for reporting aerosol optical depth statistics: empirical tests using multi-year, multi-site AERONET sunphotometer data. *Geophysical Research Letters* 27, 3333–3336.
- Pinker, R.T., Pandithurai, G., Holben, B.N., Dubovik, O., Aro, T.O., 2001. A dust outbreak episode in sub-Sahel west Africa. *Journal of Geophysical Research* 106, 22,923–22,930.
- Qiu, J.H., Yang, L.Q., 2000. Variation characteristics of atmospheric aerosol optical depths and visibility in north china during 1980–1994. *Atmospheric Environment* 34, 603–609.
- Schmid, B., Spyak, P.R., Biggar, S.F., Wehrli, C., Sekler, J., Ingold, T., Matzler, C., Kampfer, N., 1998. Evaluation of the applicability of solar and lamp radiometric calibrations of a precision sun photometer operating between 300 and 1025 nm. *Applied Optics* 37, 3923–3941.
- Schmid, B., Michalsky, J.J., Slater, D.W., Barnard, J.C., Halthore, R.N., Liljegren, J.C., Holben, B.N., Eck, T.F., Livingston, J.M., Russell, P.B., Ingold, T., Slutsker, I., 2001. Comparison of columnar water vapor measurements from solar transmittance methods. *Applied Optics* 40, 1886–1896.
- Smirnov, A., Holben, B.N., Eck, T.F., Dubovik, O., Slutsker, I., 2000. Cloud screening and quality control algorithms for the AERONET database. *Remote Sensing of Environment* 73, 337–349.
- Smirnov, A., Holben, B.N., Dubovik, O., O'Neill, N.T., Eck, T.F., Westphal, D.L., Goroch, A.K., Pietras, C., Slutsker, I., 2002a. Atmospheric aerosol optical properties in the Persian Gulf region. *Journal of Atmospheric Sciences* 59, 620–634.
- Smirnov, A., Holben, B.N., Kaufman, Y.M., Dubovik, O., Eck, T.F., Slutsker, I., Pietras, C., Halthore, R., 2002b. Optical properties of atmospheric aerosol in maritime environments. *Journal of the Atmospheric Sciences* 59, 501–523.
- Takamura, T., Nakajima, T., Okada, I., Uchiyama, A., Sugimoto, N., Shi, G.Y., Zhou, J., 2002. Aerosol-cloud-radiation study using the SKYNET data. The first ADEC Workshop, Tokyo, Japan; see <http://www.aeoliandust.com>.
- Tanaka, M., Nakajima, T., Shiobara, M., 1986. Calibration of a sunphotometer by simultaneous measurements of direct-solar and circumsolar radiations. *Applied Optics* 25, 1170–1176.

- Tegen, I., Hollrigl, P., Chin, M., Fung, I., Jacob, D., Penner, J., 1997. Contribution of different aerosol species to the global aerosol extinction optical thickness: estimates from model results. *Journal of Geophysical Research* 102, 23,895–23,915.
- Wang, D.L., Qiu, Q.H., 1986. Study on aerosol properties in Takaramakan Desert in spring. *Chinese Journal of the Atmospheric Sciences* 3, 278–288 (in Chinese).
- Zhang, X.Y., 2001. Source distributions, emission, transportation, deposition of asia dust and loess accumulation. *Quaternary Science* 21, 29–40 (in Chinese).
- Zhang, J.H., Mao, J.T., Wang, M.H., 2002. Analysis of aerosol extinction characteristics in different area of China. *Advances in Atmospheric Sciences* 19, 136–152.
- Zhou, Z.J., 2001. Blowing-sand and sandstorm in China in recent years. *Quaternary Science* 21, 9–17 (in Chinese).
- Zhu, X.S., Zhou, J., 1998. Determination of clear-sky columnar water vapor using solar radiometer. *Chinese Journal of the Atmospheric Sciences* 22, 39–45 (in Chinese).